Structure of aminopeptidase N from *Escherichia coli* suggests a compartmentalized, gated active site

Anthony Addlagatta, Leslie Gay, and Brian W. Matthews*

Howard Hughes Medical Institute and Institute of Molecular Biology and Department of Physics, University of Oregon, Eugene, OR 97403-1229

Contributed by Brian W. Matthews, July 20, 2006

Aminopeptidase N from *Escherichia coli* is a major metalloprotease that participates in the controlled hydrolysis of peptides in the proteolytic pathway. Determination of the 870-aa structure reveals that it has four domains similar to the tricorn-interacting factor F3. The thermolysin-like active site is enclosed within a large cavity with a volume of 2,200 Å^3, which is inaccessible to substrates except for a small opening of approximately 8–10 Å. The substrate-based inhibitor bestatin binds to the protein with minimal changes, suggesting that this is the active form of the enzyme. The previously described structure of F3 had three distinct conformations that were described as ''closed,'' ''intermediate,'' and ''open.'' The structure of aminopeptidase N from *E. coli*, however, is substantially more closed than any of these. Taken together, the results suggest that these proteases, which are involved in intracellular peptide degradation, prevent inadvertent hydrolysis of inappropriate substrates by enclosing the active site within a large cavity. There is also some evidence that the open form of the enzyme, which admits substrates, remains inactive until it adopts the closed form.

bestatin | closed active site | thermolysin-like protease

Protein synthesis and degradation are essential and continuous functions in all living cells. In the cytosol, proteins destined for degradation are tagged, unfolded, and passed to proteosomes or other complexes that generate peptides of 7–15 aa (1, 2). Large complexes, such as Tricorn in archaea, further process these into peptides of 2–3 aa. Finally, various aminopeptidases and carboxypeptidases convert these into individual amino acids (3–5).

Aminopeptidase N (PepN) (3, 4, 6, 7) is a zinc-dependent M1-class metalloenzyme classified as a gluzincin based on the conserved active site sequence (HEXXH-X_{18}-E) (3, 4, 8). PepN is the major aminopeptidase in bacteria and accounts for 99% of the hydrolysis of substrates with Ala at the N terminus (9). Although bacterial PepNs were initially identified as Ala aminopeptidases, subsequent studies demonstrated that *Escherichia coli*, *Lactococcus lactis*, and *Streptococcus thermophilus* PepNs have the highest specificities for the basic amino acids Arg and Lys, followed by hydrophobic/uncharged residues, like Ala, Leu, Met, and Phe (4, 10). There are conflicting reports as to whether PepN has endopeptidase as well as exopeptidase activity (3, 9, 11). Based on biochemical studies, Chandu *et al*. (3) have predicted two distinctive active sites, one for the well established exopeptidase activity and a second for the presumed endopeptidase activity of *E. coli* PepN (ePepN).

Although ePepN is the major aminopeptidase in *E. coli*, it is not essential (12, 13). The homologous human enzyme hPepN is anchored in the plasma membrane and serves as a receptor for coronavirus and helps in its internalization (14). Elevated levels of expression of this enzyme have been associated with several cancers (15).

We have undertaken a biochemical and structural investigation of PepN to elucidate its selectivity and catalytic activity. We present the structure of ePepN in the native and the bestatin-bound forms. Based on structural and sequence comparisons, together with model-building studies, we propose a mechanism that involves large domain movements between a "closed" active form and an "open" inactive form.

Results and Discussion

Overall Structure. The structure of holo- or "native" ePepN is shown in Fig. 1*A*. Except for the first four N-terminal residues, all 870 aa could be modeled in the electron density. The protein folds into four distinct domains, the first of which, domain I (residues 1–193), adopts an envelope-like structure formed by a seven-stranded β-sheet with two smaller β-sheets packed against it on the same face. Residues Pro-5–Asp-17 at the N terminus are well ordered and extend to contact domains II and IV. Whereas the Ala-7–Arg-10 region forms several hydrogen bonds with the region of Asp-367–Glu-371 near the surface of domain II, Pro-5 forms a hydrophobic stacking interaction with the side chain of Tyr-862 in domain IV.

Domain II (residues 194–443) adopts an overall thermolysin-like fold (16) and includes the active site. Based on the structure of thermolysin, this domain can be divided into two subdomains centered at Arg-307. The first subdomain is made of strands β15–β18 and helices α1 and α2, and the second subdomain is composed of helices α3–α8. These two subdomains form a deep groove that extends across the entire domain and includes the active site (Fig. 1*B*). The irregular structure in thermolysin that accommodates three of the four calcium ions is replaced by the long α4 helix (Arg-337–Ala-357) in ePepN. Because of this change, the active-site cavity of ePepN widens where the C-terminal region of the substrate is bound (Fig. 1*B*).

In common with domain I, domain III (residues 444–545) also consists entirely of β-strands (β19–β25), which form two parallel β-sheets that interact with domains II and IV.

Domain IV (residues 546–870), the largest, is composed of eight pairs of α-helices (α9–α24) arranged into two layers forming an overall cone-shaped superhelical structure. The inner and outer layers of the α-helices are arranged in an antiparallel manner. At the vertex of the cone there is an opening with a diameter of 8–10 Å. Domain IV also can be divided into two subdomains with an equal number of α-helical pairs centered at Leu-725. Together, domains I and IV seal off access to the active site. The only opening to the active site in the present crystal form is the pore on the top of the cone of domain IV (Fig. 1*A*).

Bestatin Binding. ePepN, like thermolysin, belongs to the gluzincin family of proteins, which has a common HEXXHX_{18}E zinc-binding motif in the active site. In ePepN, this motif is H^{297}EYFHX_{17}KE^{320}. His-297, His-301, and Glu-320 along with a water molecule bind to the zinc ion with tetrahedral geometry.

Conflict of interest statement: No conflicts declared.

Abbreviations: PepN, aminopeptidase N; ePepN, *Escherichia coli* PepN.

Data deposition: The atomic coordinates have been deposited in the Protein Data Bank, www.pdb.org (PDB ID codes 2HPT and 2HPO).

*To whom correspondence should be addressed. E-mail: brian@uoxray.uoregon.edu.

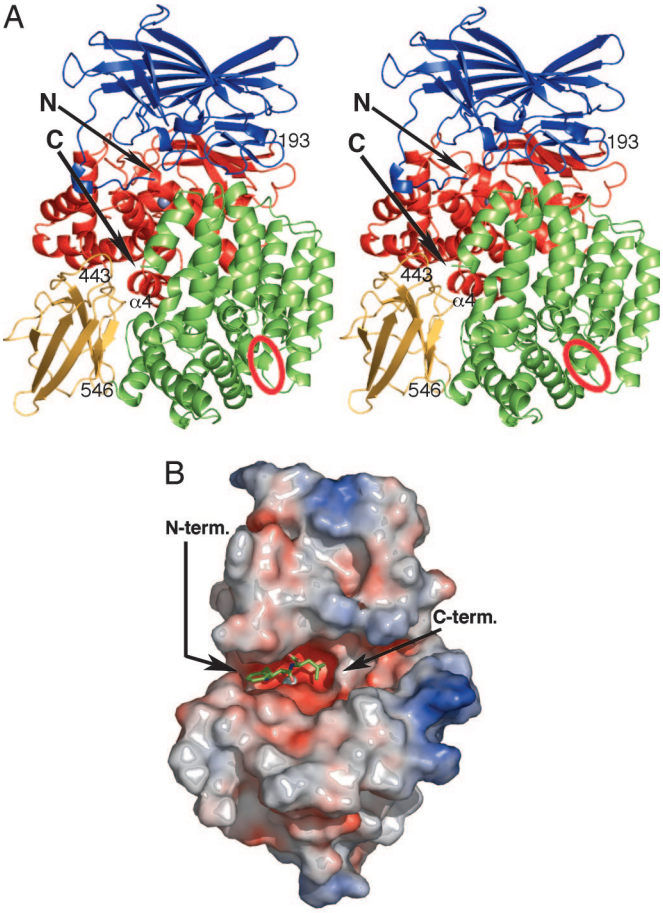

Fig. 1. Sturcture of ePepN. (*A*) Stereodiagram showing the overall structure of ePepN. Individual domains are shown in different colors: blue, domain I; red, domain II; gold, domain III; green, domain IV. The N and C termini are indicated by arrows, and the red ovals indicate the location of the small opening in domain IV. The catalytic zinc ion is blue. (*B*) Electrostatic surface diagram of the catalytic domain (domain II) of ePepN. A bestatin molecule is shown in the active site cleft, with the arrows indicating its N and C termini. The cleft is narrower on the left where the N terminus of the substrate binds and widens on the right to accommodate an extended polypeptide substrate.

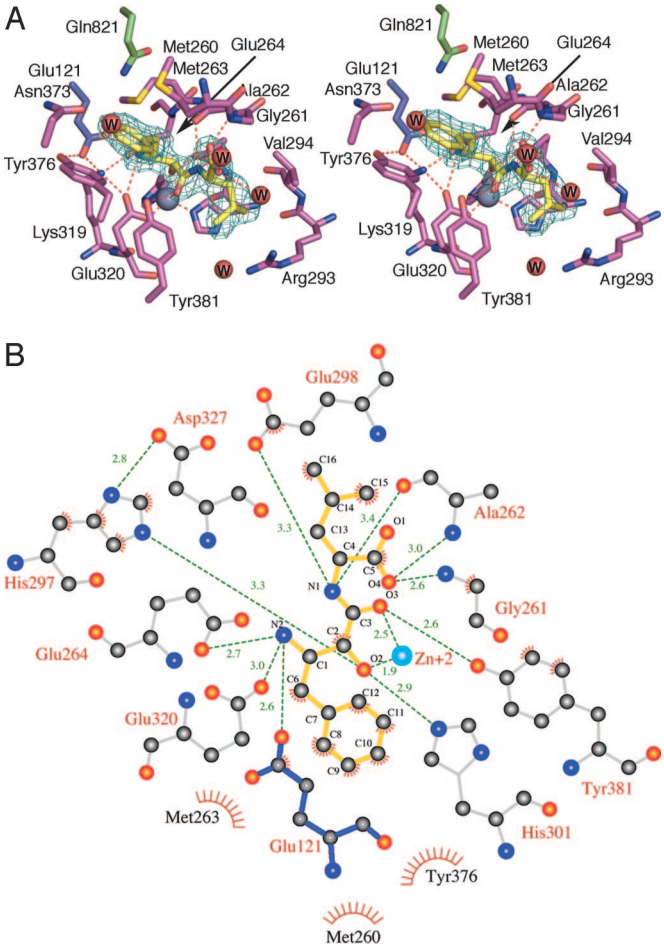

Fig. 2. Binding of bestatin to ePepN. (*A*) Bird's-eye view of the stereodiagram of bestatin bound in the active site. The electron density is a 2.3-Å resolution omit map drawn at 3.9 σ. Bestatin is shown in yellow. Residues from the catalytic domain are pink, those from domain I are blue, and those from domain IV are green. Four water molecules are represented as red spheres, and Zn^{II} is represented as a blue sphere. (*B*) LIGPLOT diagram (36) of bestatin (yellow bonds) bound to ePepN. Residues from the catalytic domain are represented in gray, and Glu-121 from domain I is blue. Zn^{II} is represented as a cyan sphere. The dashed lines indicate hydrogen bonds, and the spikes represent hydrophobic interactions.

As anticipated for the binding of bestatin to a metalloprotease, the hydroxyl group (O2) and the carbonyl group (O3) are coordinated to the zinc ion. The α-amino group points into a depression formed by Glu-121, Glu-264, and Glu-320 and forms hydrogen bonds with all three acidic groups (Fig. 2). One side of the phenylalanyl side chain of the inhibitor stacks against the side chain of Tyr-376. On the other side, Met-260, Met-263, and the CB and CG atoms of Glu-121 form a hydrophobic pocket. Residues 261–265, which include Met-263, form the so-called GAMEN substrate specificity motif common to many exopeptidases (17). The main-chain carbonyl group (O3) of bestatin, apart from interacting with the zinc ion, also forms a hydrogen bond (2.6 Å) with the hydroxyl of Tyr-381. The backbone carbonyl of Ala-262 and the side-chain carboxylate of Glu-298 interact with the N1 atom. Main-chain amides of Gly-261 and Ala-262 (from the G^{261}AMEN motif) form hydrogen bonds with one of the carboxylate atoms (O4) of the C terminus of bestatin (Fig. 2). Two water molecules form hydrogen bonds with the other oxygen atom (O1) of the carboxylate. Arg-783 and Arg-825 from domain IV are pointed into the active site and interact with the C terminus of the inhibitor through these water molecules. The leucyl side chain of the inhibitor points into a rather open hydrophobic cleft lined by Val-294, Val-324, Tyr-381, and the lateral face of the guanidyl group of Arg-293. Binding of bestatin does not change the overall structure of ePepN, although several residues that line the binding pocket undergo changes in their side-chain conformations. Met-260, which makes a hydrophobic contact with the phenyl ring of the inhibitor, moves away from its position in the native structure to make way for the bestatin. Asn-373 undergoes a change in side-chain conformation that brings its side-chain carbonyl close to the phenyl group (3.4 Å). Tyr-381, which forms a short hydrogen bond, moves away by 0.4 Å from the active site. The movements of Met-260 and Asn-373 induce changes (≈2.0 Å) in the side chains of the residues in domain I (Glu-107) and domain IV (Gln-821), which are in close proximity.

Active Site. One striking difference between ePepN and the other thermolysin-like proteases is the presence of a Lys residue (Lys-319) in the active site. The active site usually contains an Asp residue. In ePepN, the Lys residue forms a three-centered salt-bridge network with three Glu residues: Glu-121, which extends into the active site from domain I; Glu-264, which is part

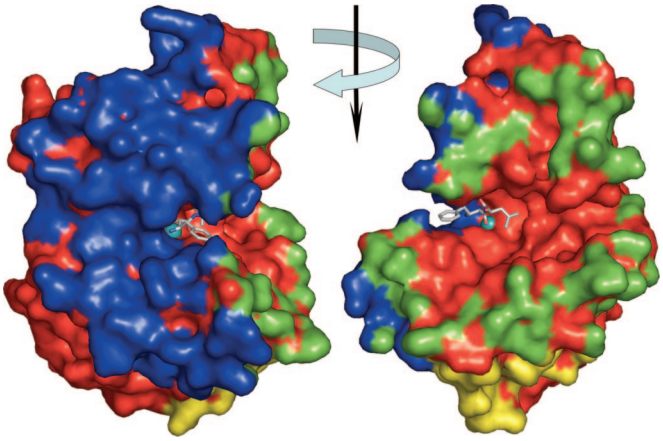

Fig. 3. Interaction surfaces between the catalytic domain (domain II) and other domains of the ePepN structure. Two views of the catalytic domain are shown, related by a 180° rotation. Bestatin is in the active site. The part of the surface colored blue is in contact with domain I, the part in green contacts domain IV, and the part in yellow contacts domain III. The remainder of domain II contacts bulk solvent and is red.

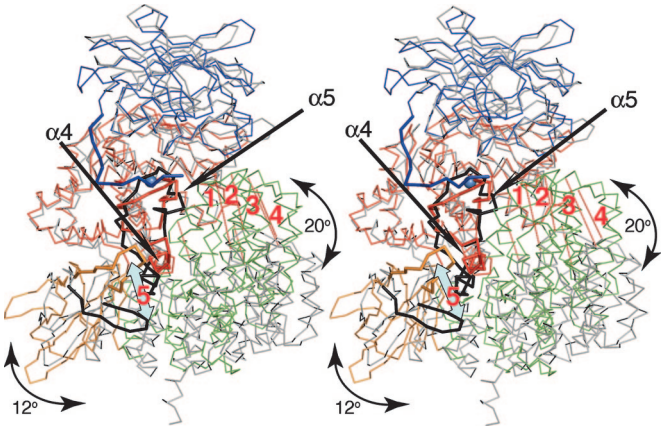

Fig. 4. Stereodiagram showing the superposition of ePepN and the F3 open structure (Protein Data Bank ID code 1Z5H, molecule A). The ePepN structure is color-coded blue, red, gold, and green for domains I, II, III, and IV, respectively. The F3 structure is gray. The C-terminal half of the α4-helix and the N terminus of α5 and the connecting loop are represented as solid lines along with a loop that undergoes a movement between the two structures. The catalytic zinc ion is blue. There are five lines in red, four of which are numbered 1–4 (also in red). These lines show the shifts in the α-helical pairs listed in Table 1. The blue double-headed arrow labeled 5 indicates a long loop in domain III that has a different conformation in F3 relative to ePepN.

of the GAME^{264}N motif; and Glu-320, which binds the active-site zinc ion. The network of the three Glu residues plus Lys form a negatively charged depression that accommodates the positively charged N terminus of the substrate (Fig. 2*A*). Glu-121 occurs in a loop at the beginning of a tight turn. While stretching into the active site, the peptide bond between Glu-121 and Ala-122 in domain I adopts a cis-configuration. Non-proline cis-peptides, which occur infrequently (0.03–0.05%), are energetically unfavorable by 2.5 kcal/mol compared with trans peptides (18).

Closed Conformation. Similar to thermolysin, the catalytic domain of ePepN is bilobal with a pronounced active site cleft at the junction of the two lobes (Fig. 1*B*). This cleft is wider and longer in ePepN because the calcium-binding loop is replaced with an α-helix as described above. Large regions of the surface of the catalytic domain interact with domains I and IV (1,966 Å^2 and 2,112 Å^2, respectively) (Fig. 3). The interactions between domains I and II are largely hydrophobic, whereas those between domains II and IV are hydrophilic. Domain I forms a wall-shaped surface that stacks against the active site on the left near the N terminus of the substrate-binding region to which it donates Glu-121. Domain IV adopts the shape of a cone, which covers the active site region in domain II.

The first subdomain (α9–α16) of domain IV contacts the far right side of the active site, whereas the second subdomain contacts the left. The second subdomain of domain IV also interacts with domain I. The combined contacts of domains I and IV with the catalytic domain results in the complete occlusion of the active site. As a consequence of this occlusion, a chamber of ≈2,200 Å^3 is created that is lined by residues from domains I, II, and IV. The only opening to the active site is at the vertex of the cone of domain IV, which has a cross-section of 8 × 10 Å (distances measured between β-carbon atoms) (Fig. 1*A*).

Chandu *et al.* (3) have suggested that ePepN has endopeptidase activity at a site distinct from the exopeptidase site. Inspection of the ePepN structure suggests that it has only a single active site. To determine whether endopeptidase activity might be feasible at this site we used model building to place the extended thermolysin inhibitor carbobenzoxy-Gly-P-Leu-Leu (16) into the ePepN structure. In such a model-built complex, there are severe steric clashes with domain I. In principle these clashes might be alleviated by moving domain I away from domain II, although this would also pull Glu-121 out of the active site. Possibly, this movement might change the specificity of substrate binding to accept the neutral amide of an extended substrate rather than a positively charged N terminus. Although there is substantial evidence for domain movement in ePepN and its relatives (see below), there is no suggestion to date that domain I can move relative to domain II.

Relationship of ePepN to Other Proteases: Closed vs. Open Structures. A search of the Protein Data Bank with DALI (19) showed that the structure of ePepN is most similar to that of the tricorn-interacting factor F3 (20). ePepN is also related to the three-domain structure of leukotrine 4A hydrolase (21).

F3 has 21% sequence identity with ePepN and, in common with ePepN, has a four-domain structure. In the crystallographic analysis of F3, three independent copies of the molecule were observed (20). In each of these copies, domains I–III plus the first half of domain IV have essentially the same structure. The second half of domain IV, however, showed relative movements of up to 15 Å. Because of these movements the three versions of the structure were classified as closed, intermediate, and open. If, for example, the open form is compared with ePepN (Fig. 4), 437 C$^\alpha$ atoms align within 1.8 Å. Comparing individual domains, domain I has 160 C$^\alpha$ atoms that align within 1.3 Å, domain II has 220 C$^\alpha$ atoms that align within 1.7 Å, domain III has 65 atoms that align within 2.2 Å, and domain IV has 188 atoms that align within 4.0 Å.

Notwithstanding the above agreement, the overall structure of ePepN differs more from F3 than any of the three copies of F3 differ among themselves. As noted above, it is the second half of domain IV of F3 that moves relative to the rest of the protein. In the case of ePepN, domains I and II are essentially the same as domains I and II of F3, but domains III and IV move substantially relative to their counterparts in F3. These movements were analyzed with DYNDOM (22). Domain III of ePepN rotated between 9° and 12° relative to its position in F3. For domain IV, the relative rotation is between 16° and 25°, the range of values reflecting the movement within this domain observed for the open forms vs. the closed forms of F3.

In going from the ePepN structure to the open form of F3, the

Table 1. Distance between helix pairs (with ePepN residue numbers in parentheses) in domain IV of F3 relative to their position in ePepN

Helix pair	Displacement of helix pair, Å		
	F3 closed	F3 intermediate	F3 open
α_{14}–α_{15} (672–706)	7.6	9.0	11.9
α_{16}–α_{17} (710–740)	8.6	10.8	14.5
α_{18}–α_{19} (761–792)	7.9	10.1	14.4
α_{20}–α_{21} (803–836)	12.9	13.5	16.3
α_{22}–α_{23} (838–870)	18.3	14.7	21.0

Distances were calculated after superimposing domains I and II of F3 on the corresponding domains in ePepN.

last five helical pairs of domain IV move away from domain II (the catalytic domain) by 12–21 Å (Fig. 4 and Table 1). This movement results in a wide opening near the surface of the protein that extends into the active site, which is at a depth of ≈28 Å. In the open form of F3, this opening measures ≈18 Å in one direction and 30 Å in the other. In going to the intermediate and closed forms, this opening is reduced in size to 15 × 30 Å and 13 × 30 Å, respectively. In the case of ePepN, the corresponding opening is, at maximum, ≈4 Å (all distances being measured between β-carbon atoms). Thus, in the ePepN structure, the active-site region is much more closed than in any of the F3 variants, including the closed form. The conformational changes that are observed for F3 indicate that the molecule is capable of substantial dynamic behavior. Extending the general argument made by Kyrieleis *et al.* (20), it is tempting to argue that ePepN also undergoes a conformational change between a closed and open form. The closed form corresponds to the crystal structure, and the open form could be similar to any of the forms of F3.

It was noted above that a loop including Glu-121 of ePepN extends from domain I into the domain II active site. In so doing, the Glu-121–Ala-122 peptide bond adopts a cis conformation. Similarly, Glu-136 of leukotrine 4A hydrolase points into the active site and the adjacent peptide bond is cis (21). There is a Glu residue in the same region of the F3 structure, but it does not point into the active site and its main chain has a normal trans configuration (20, 23).

Is the Open Substrate-Binding Site Inactive? The catalytic activity of proteases such as PepN needs to be carefully regulated. On one hand, the active site needs to be sufficiently (or transiently) open to admit appropriate substrates. On the other hand, an open active site might lead to hydrolysis of unintended substrates. It is possible that ePepN may open to admit substrates and to release products but that this open form is catalytically compromised. As discussed above, the crystal structure of ePepN corresponds to a closed form in which the active site appears to be largely if not entirely inaccessible to bulk solution. This form of the enzyme binds bestatin and combines all of the elements expected for a fully functional enzyme. In analogy with thermolysin (16), these elements include Glu-264, which helps to activate the catalytic water or hydroxide ion, and Tyr-381, which helps stabilize the tetrahedral transition state. In thermolysin, the analogous residues are Glu-240 and His-231, with the addition of Tyr-157. F3 has Tyr-351 at a site analogous to Tyr-381, as in ePepN. However, in all three structures of F3, the Tyr-351 side chain is rotated away from the zinc ion, and, in addition, the helix harboring Tyr-351 is shifted ≈2.7 Å away from the zinc ion (Fig. 5). This shift suggests that all three versions of the F3 crystal structure represent inactive conformation. Kyrieleis *et al.* (20) suggest that the active conformation is induced by substrate binding.

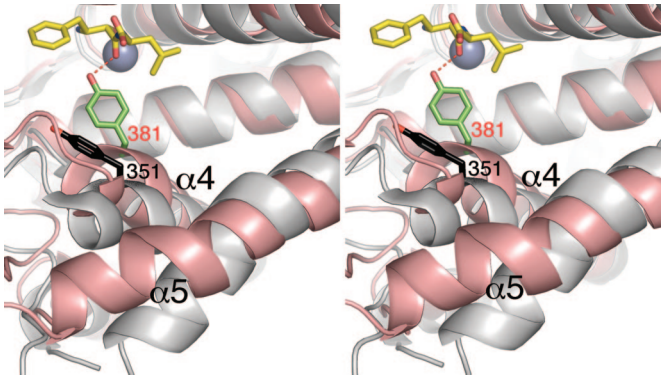

Fig. 5. Close-up stereoview of the superposition of the closed ePepN (red ribbons) and open F3 (gray) active sites. Helices α4 and α5 of the F3 structure bend away from the active site, and, in so doing, Tyr-351 of F3 (black) rotates away from the active site represented by bestatin (yellow) and zinc ion (blue). In the closed ePepN–bestatin complex, the analogous residue, Tyr-381, points into the active site and interacts with the inhibitor.

We propose that it is not substrate binding, *per se*, that activates F3 but rather a further closing of the structure toward the conformation seen for ePepN. Comparison of the structure of F3 and ePepN suggests that this closing step would induce a bend of ≈30° in the central helix (α4) of the thermolysin-like domain. This bend would bring the C terminus of the α4 helix (residues Gly-319–Ser-325 in F3) closer to the active site and, in concert, cause a 22° bend in helix α5, which would also bring its N terminus closer to the active site (residues Glu-348–Gly-352) (Fig. 5). As a consequence of this bending, the backbone of Tyr-351 in F3 would be brought ≈2 Å closer to the active site and the side chain would be directed toward the zinc ion. Requiring that the active site region be fully closed to confer catalytic activity would avoid inappropriate cleavage of proteins or peptides.

We cannot rule out the possibility that ePepN does not undergo large-scale conformational change and that substrates enter through the small opening at the vertex of the domain IV cone. The size of this opening, ≈8–10 Å, suggests that it might better allow smaller products to leave rather than longer substrates to enter. A "pore" with a maximal size of 10 Å has been proposed to serve as an entry point to the peptides in the dodecameric tetrahedral-shaped aminopeptidase (24). Such an opening into the active site chamber also has been observed in other multimeric protease structures (25). If the small opening acts as an entry point for peptides, the ePepN structure represents a class of protease that has a buried active site in a monomeric form.

Materials and Methods

Protein Cloning, Expression, Purification, and Crystallization. The gene encoding ePepN was PCR-amplified from the genomic DNA of K12 *E. coli* strain by using the forward (5′-GGAATTCCATATGACTCAACAGCCACAAGCCAAA-TACC-3′) and reverse (5′-CCGCTCGAGTCAAGCCAGT-GCTTTAGTTATCTTCTCG-3′) primer, followed by insertion into PET15b (Novagen, Darmstadt, Germany) vector between NdeI and XhoI (New England Biolabs, Ipswich, MA) restriction sites introducing an N-terminal His-tag. BL21 (DE3) bacterial cells (Novagen) were used for the expression of the protein. Cells were cultured in LB media at 37°C to an A_{600} of 1.5 before the temperature was reduced to 25°C, after which the protein expression was induced by 1 mM isopropyl β-D-thiogalactoside. Cells were harvested after 12 h by centrifuging at 8,000 × *g* for 20 min, followed by resuspension in +T/G buffer (50 mM

Table 2. X-ray data collection and refinement statistics

Parameters	Native	Bestatin	SeMet		
			Peak	Inflection	Remote
Data collection					
Space group	$P3_121$	$P3_121$	$P3_121$		
Wavelength, Å	0.95	1.00	0.9797	0.9798	0.9612
Cell parameters					
a and *b*, Å	120.44	120.67	120.88	120.89	120.90
c, Å	170.56	170.84	170.75	170.75	170.76
Resolution range, Å	20–1.65 (1.68–1.65)	20–2.30 (2.38–2.3)	20–2.25 (2.33–2.25)	20–2.25 (2.33–2.25)	20–2.25 (2.33–2.25)
R_{sym}, %	5.2 (42.3)	6.8 (36.3)	7.8 (25.8)	6.9 (13.9)	6.4 (12.4)
$I/\sigma(I)$	13.5 (1.9)	13 (6.1)	17.8 (11.8)	18.7 (12.8)	19.5 (14.5)
Completeness, %	95.5 (89.2)	100 (100)	97.7 (98.6)	97.7 (98.6)	97.6 (98.6)
Redundancy	3.2 (2.8)	8.4 (8.4)	7.0 (7.0)	7.0 (7.0)	7.0 (6.9)
Refinement					
No. of reflections	141,770	61,131			
R_{work}/R_{free}, %	16.1/18.5	15.2/19.9			
rms deviations					
Bond lengths, Å	0.01	0.02			
Bond angles, °	1.2	1.6			

Values in parentheses are for the highest resolution shell.

Hepes, pH 8.0/0.5 M KCl/10% glycerol/0.1% Triton X-100/5 mM imidazole) and lysed by being passed through a French press. After centrifugation at 17,000 × *g* for 30 min, the supernatant was applied to a talon column (cobalt affinity resin; BD Biosciences, Franklin Lakes, NJ), which was preequilibrated with +T/G buffer. Continued application of +T/G buffer was used to wash the column until the absorption at A_{280} reached the baseline. The column was further washed with −T/G buffer (50 mM Hepes, pH 8.0/0.5 M KCl/5 mM imidazole). Pure protein was eluted with 100 mM imidazole in −T/G buffer at 15 mg/ml and dialyzed twice in 4 liters of 25 mM Hepes, pH 7.5/150 mM KCl. No further purification was done either for the enzyme activity assays or for crystallization. A similar method was used to purify the selenomethionine protein. We obtained an average of 300 mg of protein from 4 liters of culture for the native enzyme. For the selenomethionine protein, the yield was ≈100 mg. The terminal His-tag was left intact for structural studies.

Protein concentration was adjusted to 11 mg/ml before setting up crystallization screens at 25°C. Initial crystals appeared within 12 h. After optimization, crystals in trigonal space group $P3_121$ were obtained in hanging drops with 5 μl of reservoir solution (1.8 M sodium malonate, pH 7.5) (Table 2). Crystals with an average size of 150 μm^3 were equilibrated for 5 min in 22% glycerol/2.0 M sodium malonate before being frozen in liquid nitrogen. Selenomethionine crystals were also grown and frozen in similar conditions. Crystals in complex with bestatin were obtained by cocrystallization under similar conditions in the presence of the ligand at 1 mM.

Data Collection. Native data and the MAD data were collected on beamline 8.2.2 at the Advanced Light Source (Lawrence Berkeley National Laboratory, Berkeley, CA) by using a Quantum 315 ADSC Area Detector (Area Detector Systems Corp., Poway, CA). Native data were collected to a resolution of 1.65 Å. Multiwavelength data were collected on the selenomethionine protein crystals to a resolution of 2.3 Å (Table 2). A 0.3° oscillation was adopted over a range of 120°. Inverse beam data were collected for every 4.8° rotation to measure the Bijvoet-related reflections. All of the data were collected simultaneously. Diffraction images were processed and scaled with HKL2000 (26).

Structure Solution and Refinement. The SHELX (27) program suite was used to search for the positions of the selenium atoms. Of the expected 21 atoms, 20 were located in anomalous difference maps along with a peak for the active site zinc. Automated model building in the 1.65-Å resolution map was done by using ArpWarp (28). The resulting model was examined and completed in O and COOT (23, 29). Structure refinement to 1.65-Å resolution (Table 1) was done by using CNS and the CCP4 program suite (30, 31). Geometric parameters for bestatin were obtained from the HIC-UP server (32). The quality of the final models was judged with PROCHECK (33). The DALI server was used to search for the structural similarities (19). Structure figures were generated by using the program PYMOL (34).

Note. While this manuscript was in preparation, the crystallization of ePepN was reported (35), and the coordinates for PepN from *Neisseria meningitides* were deposited in the Protein Data Bank (ID code 2GTQ).

We thank Xiaokun Shu and Drs. Blaine Mooers and Mohammad Yousef for assistance in measuring parts of the x-ray data and Dr. Zac Wood for fruitful discussions.

1. Graham, S. C., Lilley, P. E., Lee, M., Schaeffer, P. M., Kralicek, A. V., Dixon, N. E. & Guss, J. M. (2006) *Biochemistry* **45,** 964–975.
2. Wang, E. W., Kessler, B. M., Borodovsky, A., Cravatt, B. F., Bogyo, M., Ploegh, H. L. & Glas, R. (2000) *Proc. Natl. Acad. Sci. USA* **97,** 9990–9995.
3. Chandu, D., Kumar, A. & Nandi, D. (2003) *J. Biol. Chem.* **278,** 5548–5556.
4. Chandu, D. & Nandi, D. (2003) *Microbiology* **149,** 3437–3447.
5. Franzetti, B., Schoehn, G., Hernandez, J. F., Jaquinod, M., Ruigrok, R. W. & Zaccai, G. (2002) *EMBO J.* **21,** 2132–2138.
6. McCaman, M. T., McPartland, A. & Villarejo, M. R. (1982) *J. Bacteriol.* **152,** 848–854.
7. Niven, G. W., Holder, S. A. & Stroman, P. (1995) *Appl. Microbiol. Biotechnol.* **44,** 100–105.
8. Hooper, N. M. (1994) *FEBS Lett.* **354,** 1–6.
9. Lazdunski, C., Busuttil, J. & Lazdunski, A. (1975) *Eur. J. Biochem.* **60,** 363–369.
10. Christensen, J. E., Dudley, E. G., Pederson, J. A. & Steele, J. L. (1999) *Antonie Van Leeuwenhoek* **76,** 217–246.
11. McCaman, M. T. & Villarejo, M. R. (1982) *Arch. Biochem. Biophys.* **213,** 384–394.
12. Latil, M., Murgier, M., Lazdunski, A. & Lazdunski, C. (1976) *Mol. Gen. Genet.* **148,** 43–47.
13. Yen, C., Green, L. & Miller, C. G. (1980) *J. Mol. Biol.* **143,** 21–33.
14. Yeager, C. L., Ashmun, R. A., Williams, R. K., Cardellichio, C. B., Shapiro, L. H., Look, A. T. & Holmes, K. V. (1992) *Nature* **357,** 420–422.
15. Bauvois, B. & Dauzonne, D. (2006) *Med. Res. Rev.* **26,** 88–130.

16. Matthews, B. W. (1988) *Acct. Chem. Res.* **21,** 333–340.
17. Vazeux, G., Iturrioz, X., Corvol, P. & Llorens-Cortes, C. (1998) *Biochem. J.* **334,** 407–413.
18. Jabs, A., Weiss, M. S. & Hilgenfeld, R. (1999) *J. Mol. Biol.* **286,** 291–304.
19. Holm, L. & Sander, C. (1994) *Proteins* **19,** 165–173.
20. Kyrieleis, O. J., Goettig, P., Kiefersauer, R., Huber, R. & Brandstetter, H. (2005) *J. Mol. Biol.* **349,** 787–800.
21. Thunnissen, M. M., Nordlund, P. & Haeggstrom, J. Z. (2001) *Nat. Struct. Biol* **8,** 131–135.
22. Lee, R. A., Razaz, M. & Hayward, S. (2003) *Bioinformatics* **19,** 1290–1291.
23. Emsley, P. & Cowtan, K. (2004) *Acta Crystallogr. D* **60,** 2126–2132.
24. Russo, S. & Baumann, U. (2004) *J. Biol. Chem.* **279,** 51275–51281.
25. Borissenko, L. & Groll, M. (2005) *J. Mol. Biol.* **346,** 1207–1219.
26. Otwinowski, Z. & Minor, W. (1997) in *Methods in Enzymology*, Macromolecular Crystallography, ed. Sweet, R. M. (Academic, New York), Vol. 276, pp. 307–326.
27. Sheldrick, G. M. & Schneider, T. R. (1997) *Methods Enzymol.* **277,** 319–343.
28. Perrakis, A., Morris, R. & Lamzin, V. S. (1999) *Nat. Struct. Biol.* **6,** 458–463.
29. Jones, T. A., Zou, J. Y., Cowan, S. W. & Kjeldgaard, M. (1991) *Acta Crystallogr. A* **47,** 110–119.
30. Brunger, A. T., Adams, P. D., Clore, G. M., DeLano, W. L., Gros, P., Grosse-Kunstleve, R. W., Jiang, J. S., Kuszewski, J., Nilges, M., Pannu, N. S., *et al.* (1998) *Acta Crystallogr. D* **54,** 905–921.
31. CCP4: Collaborative Computational Project Nr4 (1994) *Acta Crystallogr. D* **50,** 760–763.
32. Kleywegt, G. J. & Jones, T. A. (1998) *Acta Crystallogr. D* **54,** 1119–1131.
33. Laskowski, R. A., Moss, D. S. & Thornton, J. M. (1993) *J. Mol. Biol.* **231,** 1049–1067.
34. DeLano, W. L. (2002) The PyMOL Molecular Graphics System (DeLano Scientific, San Carlos, CA).
35. Onohara, Y., Nakajima, Y., Ito, K., Xu, Y., Nakashima, K., Ito, T. & Yoshimoto, T. (2006) *Acta Crystallogr. F* **62,** 699–701.
36. Wallace, A. C., Laskowski, R. A. & Thornton, J. M. (1995) *Protein Eng.* **8,** 127–134.